Monthly Notices
of the
ROYAL ASTRONOMICAL SOCIETY

Mon. Not. R. Astron. Soc. **412,** 2040–2051 (2011) doi:10.1111/j.1365-2966.2010.18083.x

On the first ν_6 anti-aligned librating asteroid family of Tina

V. Carruba[1]★ and A. Morbidelli[2]

[1]*UNESP, Univ. Estadual Paulista, Grupo de dinâmica Orbital e Planetologia, Guaratinguetá, SP 12516-410, Brazil*
[2]*Université de Nice Sophia Antipolis, CNRS, Observatoire de la Côte d'Azur, Laboratoire Cassiopée, BP 4229, 06304, Nice Cedex 4, France*

Accepted 2010 November 23. Received 2010 November 18; in original form 2010 August 27

ABSTRACT

Asteroid families are groups of bodies identified in the space of proper elements or of frequencies that share a common origin in the collisional break-up of their progenitors. Their dynamical evolution is shaped by the interaction with the local web of mean-motion and secular resonances, and by non-gravitational effects, such as the 'Yarkovsky' and 'Yarkovsky–O'Keefe–Radzievskii–Paddack' (YORP) effects. Thus, obtaining information on their age and original ejection velocity field is generally a difficult task. Recently, two families were found to have a large fraction of members in the non-linear secular resonance z_1: the Agnia and Padua families. Conserved quantities of the $z_1$resonance allowed for a more precise determination of their ages and ejection velocity fields. So far, however, no family was known to be in a linear secular resonance, such as the ν_6 resonance, although individual asteroids were known to be in ν_6 anti-aligned librating states. The ν_6 resonance occurs when there is a commensurability between the frequency of precession of the pericentre of an asteroid and that of Saturn. As a consequence, in librating states, the resonant argument oscillates around a stable point. In anti-aligned librating states, the resonant argument oscillates around the stable point at 180°. Here we show that the newly identified Tina family is characterized by having all its members in such a state, making it the only family in the asteroid belt known to be completely embedded in a secular resonance configuration. This rare dynamical configuration limits the maximum eccentricity of Tina members, preventing them from experiencing Martian close encounters and forming a stable island of a new dynamical type. The current dispersion of asteroid resonant elements suggests that the family should be at least 2.5 Myr old, while Monte Carlo simulations including the Yarkovsky and YORP effects suggest that the Tina family should be 170^{+20}_{-30} Myr old.

Key words: celestial mechanics – minor planets, asteroids: general.

1 INTRODUCTION

Asteroid families are groups of small bodies that share a common collisional origin. They form clusters in the space of proper elements (a, e, $\sin(i)$) (semimajor axis, eccentricity and sine of the inclination, Zappalà et al. 1995; Bendjoya & Zappalà 2002) or proper frequencies ($n, g, g + s$) [mean motion (n) and frequency of precession of the argument of the pericentre (g) and of the longitude of the node (s), Carruba & Michtchenko 2007, 2009]. Sometimes resonant proper elements are also used, as for the Schubart and Hilda families in the 3:2 mean-motion resonance with Jupiter (denoted by $3J{:}-2A$ hereinafter, Brož & Vokrouhlický 2008), and for the youngest asteroid families, one may also use the osculating elements (for instance, the cases of the Datura and Emilkowalski families, Nesvorný & Vokrouhlický 2006). The current orbital locations of family members are, however, different from the one observed at the family formation. Family members interacted with the local web of mean-motion and secular resonances, migrated due to the effect of non-gravitational forces, such as the Yarkovsky and Yarkovsky–O'Keefe–Radzievskii–Paddack (YORP) effects, and, in some cases, experienced close encounters with massive asteroids. Since the current orbital position depends on both the original location of family members and the time when the asteroid evolved since the family formation, obtaining reliable estimates for the family ages is quite difficult and subject to a degree of uncertainty.

Secular resonances occur when there is a commensurability between the precession frequency of the asteroid longitude of the pericenter g or node s and the precession frequencies of the planets g_2, g_3, g_4, g_5, g_6, g_7, g_8 and s_2, s_3, s_4, s_6, s_7, s_8, where the suffixes 2, 3, 4, 5, 6, 7 and 8 stand for Venus, Earth, Mars, Jupiter, Saturn, Uranus and Neptune, respectively. They are distinguished between linear resonances, such as the ν_6 resonance, which occurs when $g - g_6 = 0$, the ν_5 resonance ($g - g_5 = 0$) and the ν_{16} resonance

★E-mail: vcarruba@feg.unesp.br

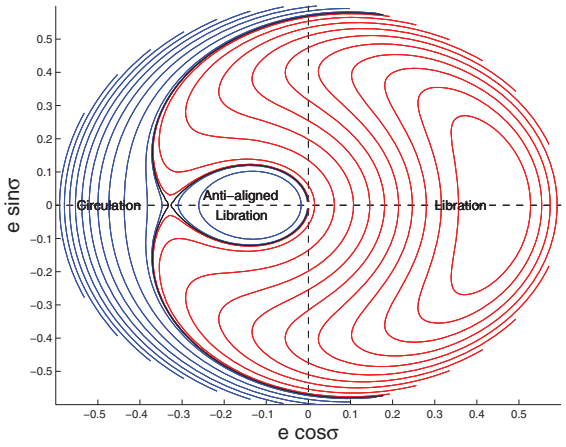

Figure 1. A diagram of equi-Hamiltonian curves for $a = 2.6$ au in the $(e\cos\sigma, e\sin\sigma)$ plane, computed for $i = 18.^{\circ}8$ (at $e = 0$) using the analytical model of Morbidelli & Henrard (1991). Circulating orbits are shown in blue, while librating orbits are shown in red. The black line displays the separatrix.

$(s - s_6 = 0)$, and non-linear ones, such as the $z_1 = \nu_6 + \nu_{16}$ resonance $(g - g_6 + s - s_6 = 0)$, that are in many cases combinations of the linear resonances (Williams 1969; Milani & Knežević 1994). Among linear secular resonances, the ν_6 resonance is among the most prominent ones in the asteroid belt, being very effective in increasing asteroid eccentricities to Mars-crossing and Earth-crossing levels.

Several asteroid families interact with secular resonances, but so far only few groups were found to have a large fraction of their members in resonant configurations. For example, two families – Agnia (Vokrouhlický et al. 2006b) and Padua (Carruba 2009a) – have been found to have the majority of their members librating in the z_1 resonance. Constraints provided by conserved quantities of this resonance allowed to obtain accurate estimates of the family ages and original ejection velocity fields. Another clump of objects around (6246) Koromotoru was found (Carruba 2009b, 2010a) to reside inside the $\nu_5 + \nu_{16}$ secular resonance. Apart from these families, only isolated objects (Froeschlé & Scholl 1987; Morbidelli & Henrard 1991) were known to be in anti-aligned librating states inside linear secular resonances, such as the ν_6 resonance. In the dynamics of the ν_6 resonance, two classes of orbits are possible in phase space: circulators and librators. For librators, the resonant argument $\sigma = \varpi - \varpi_S$ (where ϖ is the longitude of the pericentre of the asteroid and ϖ_S that of Saturn) oscillates around a fixed value. For circulating orbits, the resonant argument varies over 360°. The regions of libration and circulation are separated by a critical curve, the separatrix, originating from the unstable point at $\sigma = 180^{\circ}$ (see Fig. 1). The critical curve makes a loop around a stable point at $\sigma = 180^{\circ}$ and, inside this loop, for orbits that do not cross the origin, a different class of libration is possible: the anti-aligned libration.

Anti-aligned librators, while characterized by a libration of the resonant argument around the stable point at $\sigma = 180^{\circ}$, are actually circulating orbits that rotate in the opposite direction of external circulators. Such orbital behaviour is predicted by analytical models of the ν_6 resonance (Morbidelli & Henrard 1991) for orbits at 2.6 au, near the location of the Tina family. The reader may note from Fig. 1 that the fact that anti-aligned librating orbits do not cross the separatrix sets an upper bound on the maximum value of eccentricity achievable by bodies on these orbits, so protecting them from close encounters with terrestrial planets.

In this paper, we show that the newly discovered Tina family (Carruba 2010b) is characterized by the fact that all its known members are currently in anti-aligned librating states around $\sigma = 180^{\circ}$. It is therefore the first case of the ν_6 anti-aligned librating family and its peculiar nature can be used to set constraints on the family age (see Section 6.1).

This paper is structured as follows. In Section 2, we discuss the peculiar resonant nature of the Tina family. In Section 3, we obtain synthetic proper elements for the ν_6 resonance and in Section 4, we show numerical results that map the region of anti-aligned librating orbits in the vicinity of the Tina family. Section 5 discusses the conserved quantities of the ν_6 resonance and how these can be used to set constraints on the original ejection velocities of Tina members. The evolution of family members under the Yarkovsky force is also discussed in this section. Section 6 deals with constraints on the family age that can be obtained by virtue of the resonant dynamics or by using Monte Carlo simulations. Section 7 discusses the case of (759) Vinifera and addresses why we do not observe any family around this ν_6 anti-aligned librator. Finally, in Section 8, we present our conclusions.

2 THE RESONANT NATURE OF THE TINA FAMILY

Recently, Carruba (2010b) computed synthetic proper elements (Knežević & Milani 2000, 2003) for highly inclined [$\sin(i) > 0.3$] numbered and multiopposition objects in the region of the Pallas and Hansa families. Based on these results, a new family in the space of proper elements (a, e, $\sin(i)$) and in the space of proper frequencies (n, g, $g + s$) was identified around (1222) Tina for the first time.

Fig. 2 shows an (a, $\sin(i)$) projection of the members of the family, as identified from the clustering of proper elements (hereinafter the 'classical family', shown as full blue dots) or from the clustering of frequencies (hereinafter the 'frequency family'; we show in green the members of the Tina frequency family that do not belong to the classical one). The black dots refer to other asteroids in the region. The vertical red lines display the location of mean-motion resonances, while the blue line shows the centre of the ν_6 resonance, computed for the eccentricity value of (1222) Tina by using the second-order and fourth-degree secular perturbation theory of Milani & Knežević (1992). We warn the reader that this secular

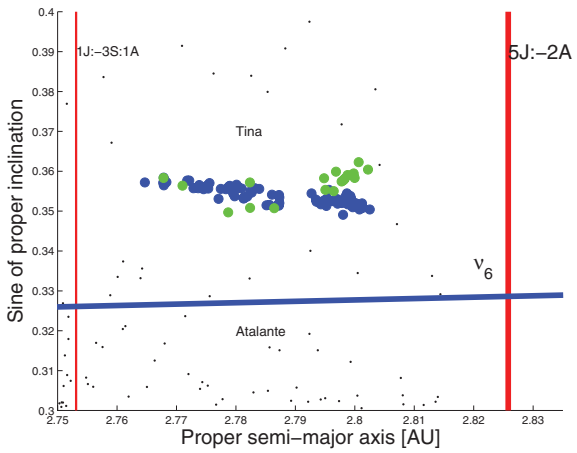

Figure 2. An (a, $\sin(i)$) projection of classical (full blue dots) and frequency (full green dots) members of the Tina families.

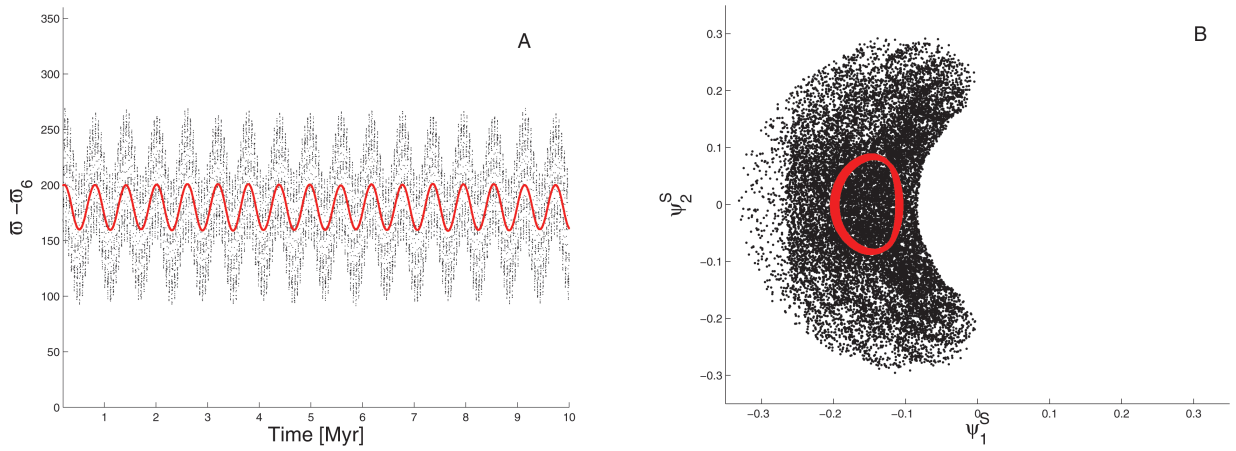

Figure 3. Panel A: the time-evolution of the resonance argument $\sigma = \varpi - \varpi_6$. The line shows the argument after being digitally filtered so as to remove all frequencies corresponding to periods less than 300 000 yr. Panel B: orbital evolution in the polar plane (ψ_1^S, ψ_2^S). The resonant elements (ψ_1^S, ψ_2^S) were also digitally filtered with the same procedure (red points).

perturbation theory loses accuracy at high inclination and close to mean-motion resonances. Thus, in Fig. 2, and in the subsequent plots, we report the location of the ν_6 resonance given by this theory just as a qualitative indication, but we do not expect it to match the distribution of the Tina family members.

It has been known since the late 1980s (Froeschlé & Scholl 1987) that (1222) Tina and the nearby asteroid, (759) Vinifera, are in an anti-aligned librating state of the ν_6 resonance. Only recently, however, fainter members of the Tina family were discovered (Carruba 2010b), while no family has yet been identified near (759) Vinifera (see Section 7). To confirm the anti-aligned librating nature of the family members, we integrated all its known 90 members of the classical and frequency families with a Burlisch–Stoer integrator modified to filter orbital elements so to eliminate all frequencies corresponding to period less than 700 yr (Brož 1999). The initial conditions of the test particles, such as inclination, longitudes of the node and pericentre, in this and all other simulations in this paper are referred to the invariable plane of the Solar system. Fig. 3 (panel A) shows the time-behaviour of the resonant argument σ for (1222) Tina. To emphasize the long-time behaviour of the angle and eliminate all short-period perturbations such as the g_5 frequency in the precession of Saturn's pericentre, the argument σ was digitally filtered so to eliminate all frequencies corresponding to periods less than 300 000 yr (see red curve, Carruba et al. 2005).

The reader may note how the resonant argument oscillates in a sinusoidal way around 180°, which is the typical behaviour for an anti-aligned oscillator. Fig. 3 (panel B) shows the orbital evolution in a polar diagram, with axes (ψ_1^S, ψ_2^S) defined as

$$\psi_1^S = \sqrt{2(1-\sqrt{1-e^2})}\cos(\varpi - \varpi_6) \quad (1)$$

and

$$\psi_2^S = \sqrt{2(1-\sqrt{1-e^2})}\sin(\varpi - \varpi_6), \quad (2)$$

respectively, where e is the asteroid eccentricity. Charlier (1902) introduced these variables (which are asymptotically equal to $e\cos\sigma$ and $e\sin\sigma$ for small e) in his theory for secular resonances. Again, black dots show the evolution with orbital elements filtered up to a period of 700 yr, while the curve shows the evolution with elements filtered up to a period of 300 000 yr. The red curve describes an oval, consistent with an anti-aligned libration (compare with Fig. 1), with period of about 50 000 yr, and the same behaviour is shared by all the 90 Tina family members. Just two other asteroids in the region, (215209) 2000 SL39 and (2002) PM7, but not connected to the family, are on anti-aligned librating orbits. While the amplitude of libration of the oscillation of the resonant argument varies among members with a maximum of 230° for 2009 NG (a member of the frequency family but not of the classical family), we found that none of the Tina asteroids was on a ν_6 circulating orbit for all the length of the integration (20 Myr).

The resonant nature of the Tina family prompts us to compute appropriate proper elements for its members with the procedure discussed in the next section.

3 SYNTHETIC PROPER ELEMENTS OF THE ν_6 RESONANCE

Synthetic proper elements are usually obtained numerically by performing a 10-Myr numerical integration (Knežević & Milani 2000). The proper semimajor axis a is then computed by averaging the osculating elements over a 2 Myr period with a running box, so as to produce 10 data points. The mean result is the proper semimajor axis and the standard deviation yields an estimate of the uncertainty of the proper semimajor axis with this procedure.

The procedure is different for the proper eccentricity e and precession frequency of the pericentre g, and for the proper inclination i and precession frequency of the longitude of the node s. The equinoctial elements $(e\cos(\varpi), e\sin(\varpi))$ and $(\sin i/2\cos(\Omega), \sin i/2\sin(\Omega))$ are Fourier analysed so as to determine the frequencies g and s associated to the largest amplitudes in the spectrum. The amplitudes associated with such frequencies are identified, respectively, with the proper eccentricity and with the sine of half the proper inclination. For a vast majority of asteroids, the frequencies of largest amplitude are the proper frequencies. However, some asteroids such as (480) Hansa are characterized by forced eccentricities larger than the free (proper) eccentricities. For these asteroids, the frequency associated with the largest amplitude in the spectrum may be one of the planetary frequencies, such as g_5 or g_6. To deal with such cases, Knežević & Milani (2000) exclude from the Fourier spectra of the equinoctial elements the terms associated with the planetary frequencies.

This procedure is not appropriate for the Tina family members, since they are currently in the ν_6 resonance and therefore their proper frequency g is very close to g_6. To deal with the special

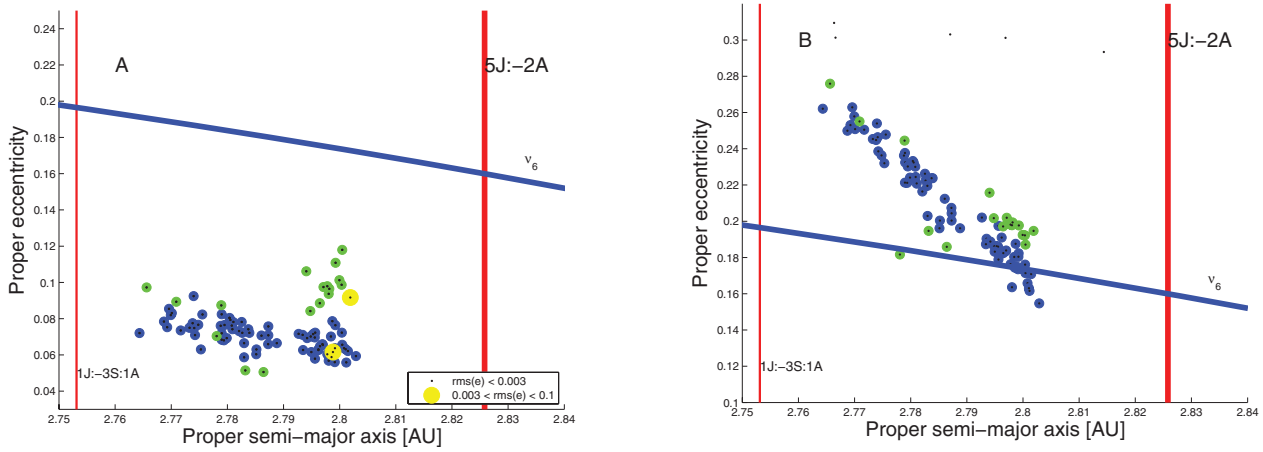

Figure 4. Panel A: a proper (a, e) projection of AstDyS asteroids in the region of the Tina family. Proper elements were obtained with the first method described in the text. Yellow circles display asteroids with standard deviation on e between 0.003 and 0.1. Panel B: a proper (a, e) projection of the same asteroids, but for proper elements obtained with the second method.

nature of the Tina asteroids, we can introduce two kinds of resonant proper elements. In the first case, we compute the resonant equinoctial elements $(e\cos(\varpi - \varpi_6), e\sin(\varpi - \varpi_6)$ filtered so as to eliminate all frequencies corresponding to periods of 300 000 yr and analyse the Fourier spectra of these new quantities. The second frequency of largest amplitude (the first is associated with the forced eccentricity of Tina asteroids) is identified with the new proper frequency (g_σ) and the amplitude associated with this frequency is identified with the new proper (or free) 'eccentricity'. For orbits in anti-aligned libration, as Tina's, g_σ is the frequency of libration and the proper eccentricity is the amplitude of libration. But, in principle, the proper eccentricity and g_σ can be defined for any orbit, even if their geometrical meaning is different. Errors on the proper e and g_σ frequencies are computed with the same method used for the traditional synthetic proper elements, while the other proper elements are still computed with the Knežević & Milani (2000) approach.

Fig. 4 (panel A) shows an (a, e) projection of asteroids in the region of the Tina family, with errors on the resonant proper e. Following the approach of Carruba (2010b), we consider 'stable' asteroids whose proper eccentricities have errors (hereinafter standard deviation-rms) smaller than 0.003. Only two asteroids in the region have unstable elements according to this definition and none of them has pathological values of rms$(e) > 0.1$. The blue line displays the location of the centre of the ν_6 resonance analytically computed for the inclination of (1222) Tina using the second-order and fourth-degree secular perturbation theory of Milani & Knežević (1992), which does not fit the distribution of the family very well. The other symbols have the same meaning as in Fig. 2. Maximum osculating eccentricities for anti-aligned asteroids are quite smaller than the minimum value necessary to experience close encounters with Mars ($e = 0.4$, obtained by equating the pericentre of an asteroid with Tina's semimajor axis with Mars' apocentre and by solving for the asteroid eccentricity).

A second approach for obtaining resonant proper elements is similar to the one used for asteroids in mean-motion resonances with Jupiter, such as the Hilda population (Brož & Vokrouhlický 2008). At the simplest level of perturbation theory, the ν_6 resonance is characterized by the conservation of the quantities $K_1 = \sqrt{a}$ and $K_2 = \sqrt{a(1-e^2)}(1-\cos i)$ (Morbidelli 2002). Obviously, K_1 and K_2 are conserved only when the sole resonant perturbations are taken into account. Non-resonant effects introduce oscillations with small amplitudes and short periods, which are removed by digital filtering of the numerical output. Here, we introduce a modified quantity $K_2' = K_2/K_1 = \sqrt{1-e^2}(1-\cos i)$ that is conserved by virtue of the conservation of K_1 and K_2. The conservation of the K_1 integral implies that the mean value of the time-series of the semimajor axis may be taken as a first proper element. The conservation of K_2' implies that oscillations of eccentricities are correlated with oscillations of inclination. One can therefore define as proper eccentricity the value of e when $\sigma = \varpi - \varpi_6 = 180^\circ$ and $\frac{\mathrm{d}\sigma}{\mathrm{d}t} > 0$, that is, the maximum value of e during the resonant cycle (Brož & Vokrouhlický 2008). Values of the proper inclination would then be obtained using the conservation of K_2'. Since this method does not allow to estimate proper frequencies, for the purpose of obtaining frequency families, we will use the elements obtained with the first method in this paper.

We applied this procedure after filtering the elements $(e\cos\sigma, e\sin\sigma)$ so as to eliminate all frequencies corresponding to periods less than 300 000 yr, which is enough to remove short-period terms, but not the terms corresponding to periods of $\simeq$700 000 yr associated with the changes in the ν_6 libration amplitudes, and results are shown in Fig. 4 (panel B). Values of eccentricities obtained with the second method are in general shifted by 0.14 relative to those computed with the first method. This is caused by the fact that in the second method, the proper eccentricity is taken as the maximum eccentricity during the libration cycle that corresponds to the sum of the eccentricity of the centre of libration (forced eccentricity) plus the radius of the libration cycle (free eccentricity). Since the first method gives as proper eccentricity the free eccentricity only, the difference between the two values of proper eccentricities is associated with the forced eccentricity of each object.

Using the two new sets of resonant proper elements and proper frequencies, we performed a new search for the members of the Tina family, using the same cut-off distance as used in Carruba (2010b). We found no difference in membership between the families found with resonant and non-resonant proper elements.

4 NUMERICAL EXPLORATION

In this section, we study the dynamics of the family and in its vicinity, using numerical tools, also including the effects of non-gravitational forces. We start by computing dynamical maps in the vicinity of the Tina family.

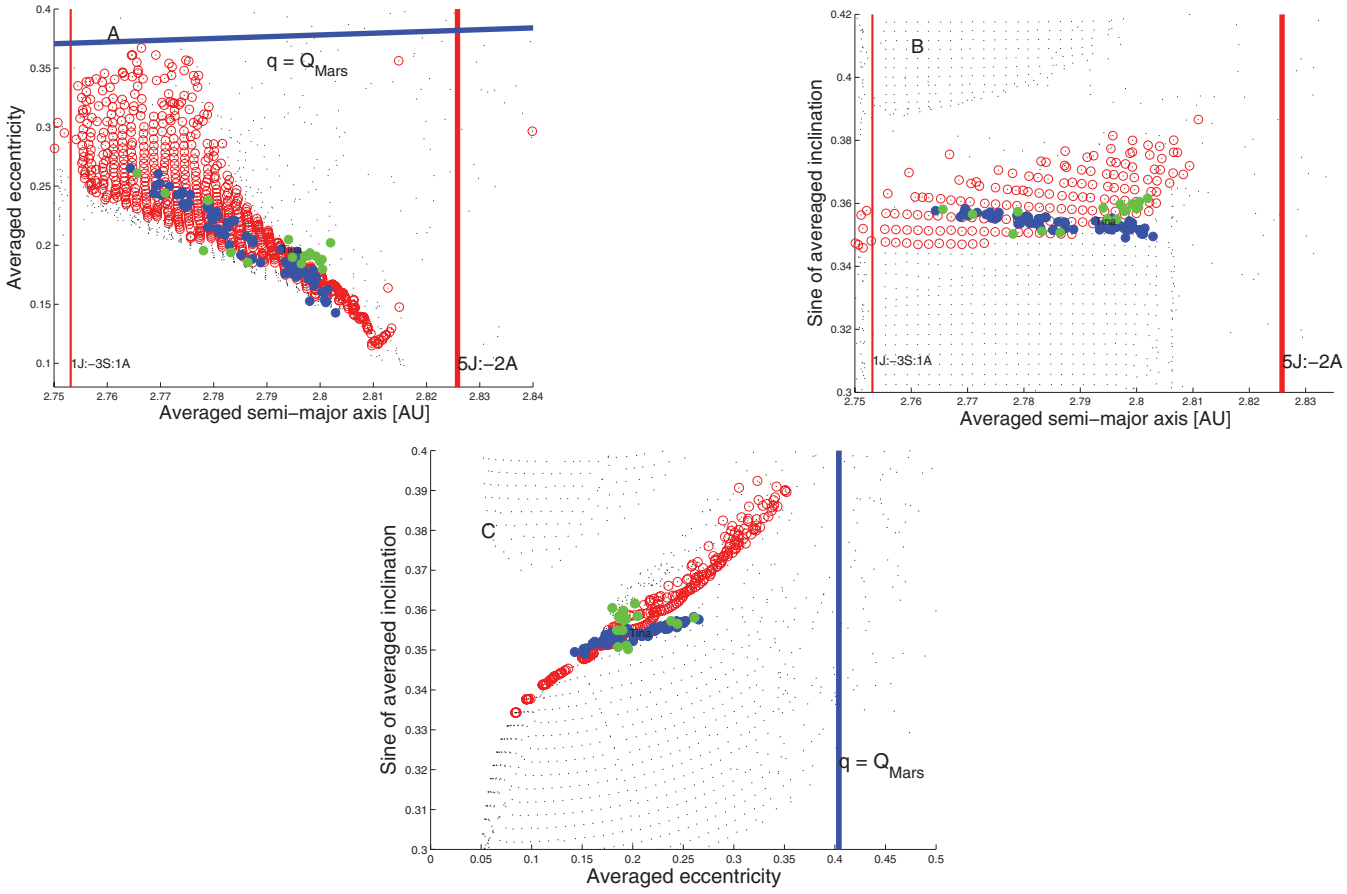

Figure 5. An (a, e) (panel A), (a, sin(i)) (panel B) and (e, sin(i)) (panel C) projection of averaged elements for test particles in the region of the Tina family.

4.1 Dynamical maps

To gain further insight into the distribution of mean-motion and secular resonances in the region, and on the orbital location of the ν_6 anti-aligned librators, we integrated with SWIFT_MVSF [the symplectic integrator of the original SWIFT package (Levison & Duncan 1994), modified by Mira Brož (1999) to account for online filtering of the osculating elements] 2400 particles in the (a, e) plane, 1600 particles in the (a, sin(i)) plane and 2400 particles in the (e, sin(i)) plane, over 20 Myr. We used a grid of 40 by 60 particles in the (a, e) plane, 40 by 40 particles in the (a, sin(i)) plane and 60 by 40 particles in the (e, sin(i)) plane, with a resolution of 0.002 au in a, 0.01 in e and 0.°2 in i. Our particles covered a range 2.75–2.83 au in a, 0–0.59 in e and 16.°0–23.°8 in i. The initial values of sin(i), e and a [for the simulations in the (a, e), (a, sin(i)) and (e, sin(i)) planes, respectively], and the initial angular elements Ω, ω and λ of the test particles were set equal to those of (1222) Tina at J2000.

Fig. 5 (panel A) displays the semimajor axis and eccentricity of the test particles averaged over the numerical simulation. Averaged elements are not constants of the motion, unlike the proper elements, but are also much simpler to compute for chaotic orbits, and can still provide qualitative insight into the local dynamics (Carruba 2009b). Red circles in the figure denote particles in anti-aligned libration and black dots denote the other particles. We do not plot any symbol for particles that did not survive for the full integration time-scale. Thus, strongly unstable regions appear empty in such a dynamical map. The red vertical lines show the location of mean-motion resonances in the region and the blue line shows the location of orbits with $q = Q_{\rm Mars}$. The full blue and green dots show the location of members of the Tina classical and frequency families, respectively. Real family members other than (1222) Tina are reported in this figure just for a qualitative comparison with the dynamical map, since their initial angles Ω, ω, M and i are not the same as those used for the map.

As can be seen in the figure, the vast majority of orbits in the region that survived the integration are anti-aligned librating particles (the red circles dominate in number over the black dots). This is due to the fact that, for anti-aligned librators, the maximum value that the eccentricity can reach over a libration cycle is small. Instead, circulating and librating orbits can easily reach Mars-crossing eccentricity values and be removed. We believe that the mechanism provided by the anti-aligned librating nature of the orbits of the Tina family members may protect these asteroids for long periods from close encounters with the terrestrial planets; we will further investigate this subject in Section 4.2, where we will be dealing with non-conservative dynamics. Note that in Fig. 5 (panel A), the region covered by red circles extends almost up to the Mars-crossing boundary ($q = Q_{\rm Mars}$ in the first approximation).

Fig. 5 (panel B) displays the averaged elements of the test particles in the (a, sin(i)) plane. The gap in the distribution of dots and circles slightly above the family illustrates the region destabilized by the ν_6 resonance (see Carruba 2010a for a discussion of the destabilizing mechanism).

Finally, Fig. 5 (panel C) displays the averaged elements of the test particles in the $(e, \sin(i))$ plane. The vertical blue line displays the value of eccentricity (0.4) needed for a particle with Tina's semimajor axis to have a pericentre equal to Mars' apocentre. Particles with $e > 0.4$ are rapidly lost because of close encounters with Mars. As can be seen in the figure, the layer of anti-aligned librators is very thin in inclination in this projection, but it still encompasses Tina and other family members.

4.2 Yarkovsky integrations

To investigate the orbital evolution over a long time-span of the members of the Tina classical and frequency families, we numerically integrated the family members with SWIFT-RMVSY, the symplectic integrator of Brož (1999) that simulates the diurnal and seasonal versions of the Yarkovsky effect. Since the Tina family seems to be made mostly of S-type asteroids (Carruba 2010b), we used values of the Yarkovsky parameters appropriate for such bodies (Carruba et al. 2003): a thermal conductivity $K = 0.001\,\mathrm{W\,m^{-1}\,K^{-1}}$, a thermal capacity $C = 680\,\mathrm{J\,kg^{-1}\,K^{-1}}$, surface density $1500\,\mathrm{kg\,m^{-3}}$, a Bond albedo of 0.1, a thermal emissivity of 0.95 and a bulk density of $2500\,\mathrm{kg\,m^{-3}}$. We used two sets of spin-axis orientations, one with an obliquity of $+90^\circ$ and the other with an obliquity of -90° with respect to the orbital plane, and periods obtained assuming that the rotation frequency is inversely proportional to the object's radius and that a 1-km asteroid had a rotation period of 5 h (Farinella, Vokrouhlický & Hartmann 1998). The radius of each body was estimated from its absolute magnitude, assuming an albedo of 0.3086, the mean value of the geometric albedo for Tina family members (Carruba 2010b).

No re-orientations were considered, so that the drift caused by the Yarkovsky effect was the maximum possible. We integrated the 182 clones of members of the classical and frequency families over 300 Myr in the future and 300 Myr in the past,[1] and computed synthetic resonant proper elements (see Section 3) for each particle every $\simeq$2.5 Myr.

Fig. 6 shows an $(a, \sin(i))$ projection of the forward time-evolution of resonant proper elements, computed with the first approach of Section 3, of the 182 clones of members of the Tina families evolving under the action of the Yarkovsky effect. Results are similar for the backward integrations. The blue and green full dots show the orbital location of the members of the classical and frequency Tina families, respectively. The vertical lines display the location of mean-motion resonances and inclined lines display the location of secular resonances. Test particles in ν_6 anti-aligned librating states are identified by red dots and test particles in ν_6 circulating or aligned librating states are shown as black dots. Each dot corresponds to the ν_6 resonant proper elements of a particle obtained over $\simeq$2.5 Myr. As can be seen in the figure, test particles evolve towards larger or smaller values of the semimajor axis under the influence of the Yarkovsky effect, until interacting with the two main mean-motion resonances in the region: the $5J{:}-2A$ two-body and the $1J{:}-3S{:}1A$ three-body resonances with Jupiter and Saturn (two particles interacted with the $\nu_6 - \nu_{16}$ secular resonance). As an effect of their interaction with mean-motion and secular resonances, test particles exited the ν_6 anti-aligned librating region and consequently increased the orbital eccentricity above Mars-crossing

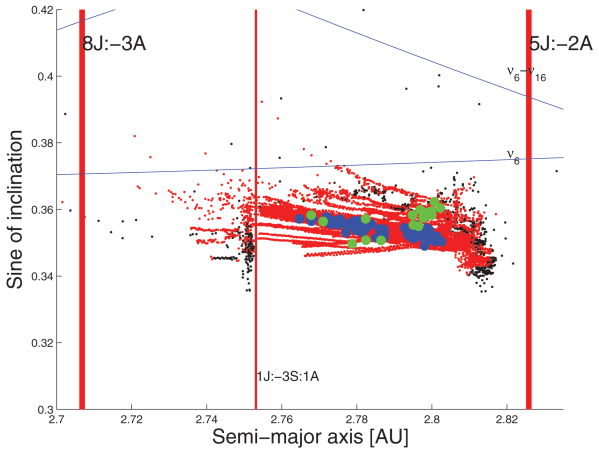

Figure 6. An $(a, \sin(i))$ projection of the forward time-evolution of resonant proper elements of the 182 clones of members of the Tina families evolving under the action of the Yarkovsky effect.

values. All these particles were lost on time-scale of 10 Myr or less (a particle was lost in our simulation if it collided with the Sun or if it had a semimajor axis larger than 100 au), which explains why there are so few black dots, corresponding to particles alive but not in an anti-aligned librating state (see Fig. 6).

Fig. 7 shows the last stages of the time-evolution of the ν_6 resonance argument σ (panel A) and osculating eccentricity (panel B) for a clone of the asteroid (211412) (2002 VL103), a typical case of an object that left the ν_6 anti-aligned state and was lost shortly afterwards. While the asteroid was in a ν_6 anti-aligned state, the maximum eccentricity reached by the asteroid never exceeded the critical value of 0.4 to encounter Mars. As soon as the test particle escaped from this state and σ started to circulate, the eccentricity quickly increased above the Mars-crossing threshold and the particle was lost in less than 4 Myr.

To quantitatively study the longevity of the Tina family, we computed the number of family members in the space of proper elements $(a, e, \sin(i))$ and proper frequencies $(n, g, g + s)$ at each time-step. We used a distance cut-off of $122\,\mathrm{m\,s^{-1}}$ in the space of proper elements and of 0.605 arcsec $\mathrm{yr^{-1}}$ in the domain of proper frequencies, as in Carruba (2010b).

Fig. 8 displays the number of the integrated Tina classical family members as a function of time. The horizontal black line shows the limit ($N_{\min} = 12$) for a group to be recognized as a clump, while the horizontal red line in panel B shows the limit for a group to be classified as a family ($N_{\mathrm{fam}} = 30$), at a velocity cut-off of $122\,\mathrm{m\,s^{-1}}$. The dashed vertical line separates the results of the integration forward in time from those of the integration backward in time. The higher the time during which the integrated clump has more than $N_{\min}$ members (hereinafter detectability time), the more likely is that the clump is a real collisional family rather than a statistical fluke. The Tina family is detectable as a group for 150–200 Myr in both the forward and the backward integrations. We repeated the same analysis for the Tina frequency family and, again, the Tina family is detectable for about 200 Myr. We conclude that the Tina family seems to be a statistically robust group, with an estimated minimum dispersion time of about 150–200 Myr. The actual dispersion time may be a factor of 2 longer, since here we used extreme obliquity values (0°, 180°) that maximize the Yarkovsky effect. Constraints on the original ejection velocities and family age will be obtained in the following sections.

[1] Yarkovsky integrations are not time-reversible. Backward integrations are equivalent to forward integrations and thus double our statistics on the family spreading as a function of time.

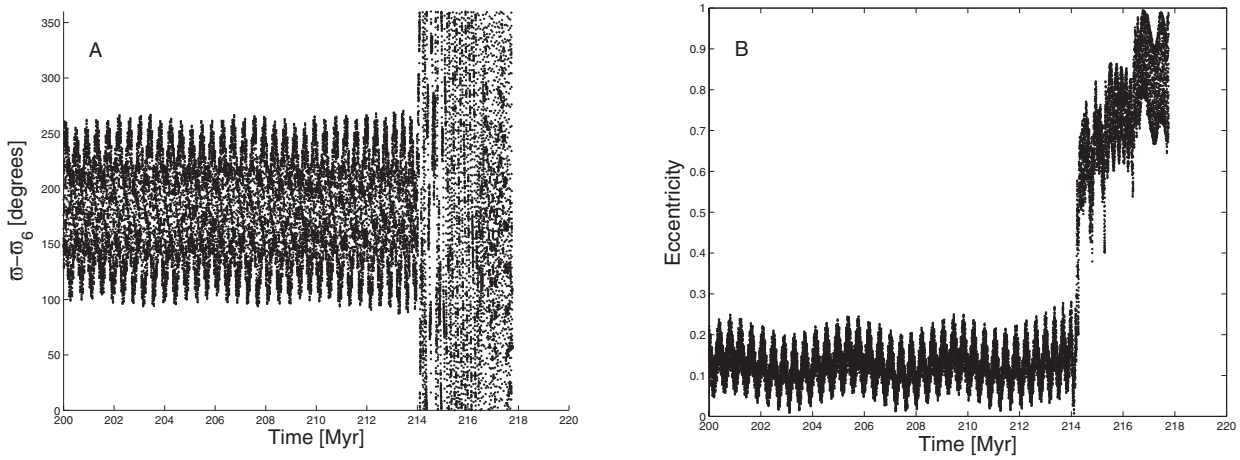

Figure 7. Panel A: the time-evolution of the osculating resonance argument $\varpi - \varpi_6$ for a clone of the asteroid (211412) (2002 VL103). Panel B: the time-evolution of the osculating eccentricity of the same test particle.

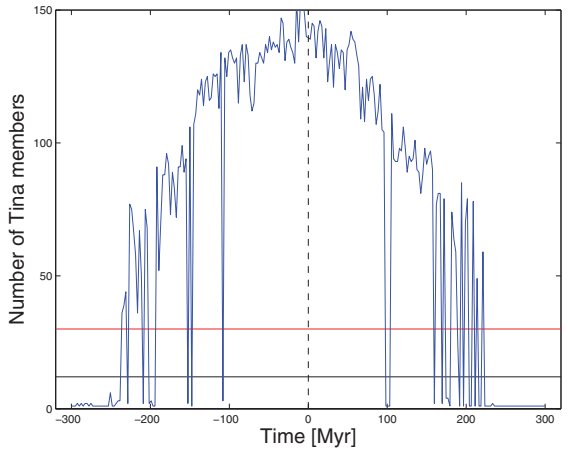

Figure 8. The number of integrated Tina family classical members as a function of time.

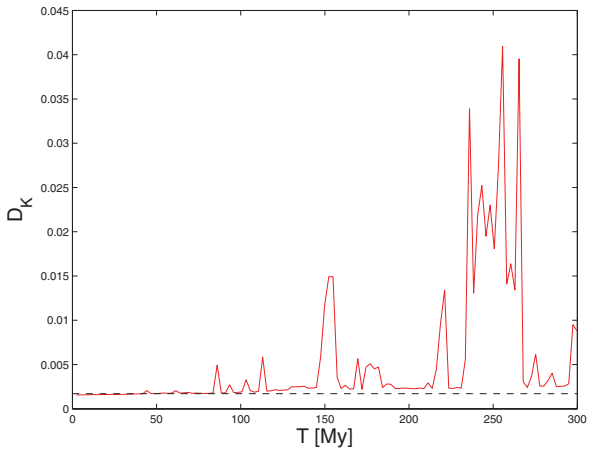

Figure 9. Value of D_K over time for the simulations that include the Yarkovsky effect. The dotted line displays the value of D_K computed on the subset of anti-aligned librating particles.

5 CONSERVED QUANTITIES OF THE ν_6 RESONANCE AND CONSTRAINTS ON THE ORIGINAL EJECTION VELOCITIES

Each resonance is characterized by one or more 'conserved quantities', which are combinations of the orbital elements that do not show any variation associated with the motion of the resonant argument. Because these quantities do not change over time, their values reflect the original values that the family had at the time of collisional break-up. This can give a valuable indication of the magnitude of the initial ejection velocity field, as shown in the cases of the families of Agnia and Padua by Vokrouhlický et al. (2006) and Carruba (2009a). Here we repeat this approach to estimate the initial ejection velocity field of the Tina family. Here, we used the conservation of the K'_2 quantity (see Section 3) for the same purpose. We computed K'_2 values for the Tina family members integrated under the action of the Yarkovsky effect. Because K'_2 does not depend on a, we expect that this quantity is almost invariant with time under the Yarkovsky effect. To quantify the time-invariance of the values of K'_2, we define a 'dispersion' D_K of the values of K'_2 as

$$D_K = \frac{1}{N(N-1)} \sum_{i \neq j} [K'_2(i) - K'_2(j)]^2, \quad (3)$$

where $N = 91$ is the number of integrated bodies and $K'_2(i)$ is the conserved quantity of the ith body ($i = 1, \ldots, N$).

Fig. 9 displays the time-evolution of D_K. As expected, D_K is nearly constant for the first 40 Myr of the simulation; fluctuations from its initial value then start to occur, because of particles escaping from the ν_6 anti-aligned region. After 150 Myr, several of the integrated family members escaped from the anti-aligned configuration and therefore the values of D_K oscillate wildly. However, if we restrict the calculation of D_K on the subset of the particles that remain in the ν_6 anti-aligned configuration, then its value remains remarkably constant (see Fig. 9, dotted line). From this experiment, we conclude that the distribution of the values of K'_2 is invariant, as long as family members do not escape from the resonance, even if the Yarkovsky effect is acting. This distribution therefore reflects the original distribution and can be used to estimate the initial dispersion velocity of the family. We do this estimation as follows.

First, we compute the distribution of the values of K'_2 for the Tina classical members with available absolute magnitude data (Fig. 10). It is a near-Gaussian distribution with a standard deviation of $\simeq 4.3 \times 10^{-4}$. Then, we construct synthetic asteroid families, where we impose that the family members are ejected relative to the family barycentre with a velocity field that is isotropic and Gaussian,

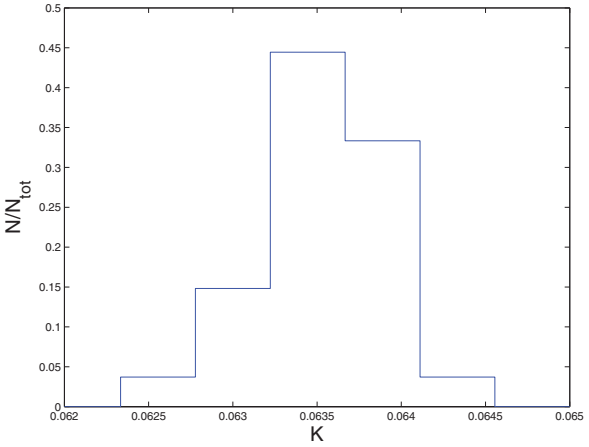

Figure 10. Normalized histogram of the distribution of the values of K'_2 for the Tina family members.

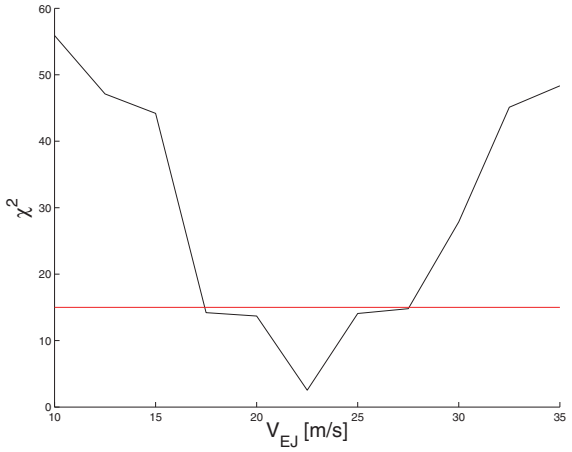

Figure 11. The values of χ^2 of the synthetic families as a function of the values of $V_{\rm EJ}$ adopted in the construction of the observed classical family.

centred around zero and with a size-dependent standard deviation that follows the relationship

$$V_{\rm SD} = V_{\rm EJ}\left(\frac{5\,{\rm km}}{D}\right), \tag{4}$$

where $V_{\rm EJ}$ is a free parameter characterizing the size of the family in velocity space and D is the asteroid diameter. We use for each synthetic family the same number of asteroids known for the Tina family and the same values of their diameters, estimated from their absolute magnitudes assuming a geometric albedo $p_V = 0.3086$ (the mean value of the geometric albedo for Tina family members, Carruba 2010b). The velocity distribution relative to the barycentre of the family is then translated into an (a, e, i) distribution by using Gauss equations (Carruba et al. 2003) and adopting for the values of Ω, ω and M the current values of (1222) Tina in the frame J2000.

Finally, for each synthetic family, we compute the distribution of the values of K'_2. We aim at determining the value of the parameter $V_{\rm EJ}$ for which the K'_2-distribution of the synthetic family best fits that of the observed family. For this purpose, for each family, we introduce a χ^2-like variable defined as

$$\chi^2 = \sum_{i=1}^{N_{\rm int}} \frac{(q_i - p_i)^2}{q_i}, \tag{5}$$

where $N_{\rm int}$ is the number of interval used for the values of K'_2 (10 equally spaced intervals, starting from $K'_2 = 0.061$ up to 0.065), q_i is the number of real objects in the ith interval in K'_2 and p_i is the number of synthetic family members in the same ith interval. We found that the distribution of K'_2 values for the synthetic family with the smallest value of χ^2 (the best-fitting family) is almost identical to the K'_2 distribution of real objects.

Fig. 11 shows how the value of χ^2 changes with the value of $V_{\rm EJ}$ adopted to generate the synthetic family. The minimal value of χ^2 (best fit) is obtained for $V_{\rm EJ} \simeq 22\,{\rm m\,s^{-1}}$. To have an estimate of the uncertainty on $V_{\rm EJ}$, we consider that, given the number of intervals (10) used for binning the distribution of K'_2, a value of $\chi^2 < 15$ corresponds to the two distributions having a probability larger than 95 per cent to be derived from the same parent distribution (Press et al. 2001). Then, we consider 'acceptable' all values of $V_{\rm EJ}$ giving $\chi^2 < 15$. This yields $V_{\rm EJ}$ of $22.5 \pm 5.0\,{\rm m\,s^{-1}}$, which is consistent with the escape velocity $V_{\rm esc} = 11.3\,{\rm m\,s^{-1}}$ from the Tina parent body, estimated using

$$V_{\rm esc} = \sqrt{\frac{2GM_{\rm Tot}}{R_{\rm PB}}}, \tag{6}$$

where G is the gravitational constant, and $M_{\rm Tot} = 0.2 \times 10^{17}$ kg and $R_{\rm PB} = 20.8$ km are the estimated mass of the family and the radius of the parent body (the values of these two parameters are taken from Carruba 2010b), respectively. An alternative way to estimate $V_{\rm EJ}$ (but providing a consistent result) will be discussed in Section 6.2.

6 CONSTRAINTS ON THE FAMILY AGE

In this section, we will set constraints on the family age by using the unique resonant configuration of the family members (Section 6.1) and by performing Monte Carlo simulations of diffusion in the semimajor axis caused by the Yarkovsky and YORP effects (Section 6.2). We will start by studying the current orbital dispersion of family members in the $(\psi_1^{\rm S}, \psi_2^{\rm S})$ plane.

6.1 Orbital dispersion in the $(\psi_1^{\rm S}, \psi_2^{\rm S})$ plane

The unique dynamical nature of the Tina family can be used to set constraints on its age. Fig. 12 shows a $(\psi_1^{\rm S}, \psi_2^{\rm S})$ projection of the current orbital distribution of the members of the classical (blue full dots) and frequency (green full dots) families. The fact that the asteroids are not clustered around a specific location in this plane but are dispersed all around the stable equilibrium point at $\sigma = 180^\circ$ suggests that the family did not form recently. In fact, reasonable ejection velocity field produced by collisional break-up events produces longitude of the pericentre and node dispersed by less than 10° (Vokrouhlický et al. 2006; Carruba 2009a). Thus, at the family formation time, the family members should be clustered in σ within a comparable dispersion. Then, the distribution in σ spreads with time, because each asteroid has a slightly different frequency of libration, g_σ, and eventually the σ distribution has to be uniform. The time it takes to achieve such a uniform distribution sets a lower limit on the age of the Tina family that we evaluate below.

To quantitatively estimate the rate at which the Tina family disperses along the σ-libration cycles, we performed the following numerical experiment: we started with a synthetic Tina family generated as a compact cluster in $a, e, \sin(i), \psi_1^{\rm S}$ and $\psi_2^{\rm S}$. To better define

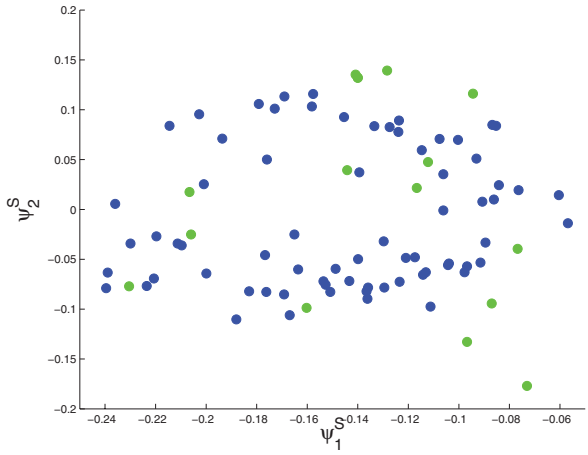

Figure 12. Projection in the (ψ_1^S, ψ_2^S) plane of the Tina family members at $t = 0$ Myr. Members of the classical family are shown as blue full dots, while members of the frequency family that do not belong to the classical family are displayed as green full dots.

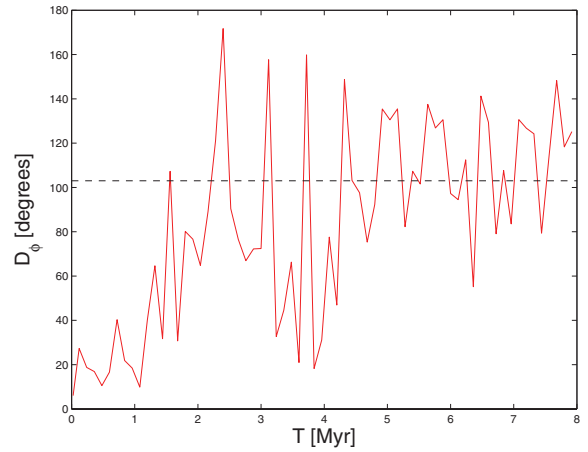

Figure 13. Time-evolution of the polar angle dispersion for the synthetic Tina family.

the spreading time along the libration cycles, the fake family is composed of a subgroup of eight observed Tina family members with values of σ to within 10°, and four sets of clones produced by adding and subtracting small values of the eccentricities and inclination of the real objects. The stable point of libration depends on the proper values of (a, i) of each object and is slightly different for different asteroids. We chose eight Tina members characterized by similar values of the location of the libration point and averaged the values of ψ_1^S and ψ_2^S of these objects. The stable point for these eight objects has coordinates $(-0.16, 0)$ in the (ψ_1^S, ψ_2^S) plane. Overall, we integrated 40 clones of Tina members. To quantitatively describe the distribution of bodies around the stable $\sigma = 180°$ point, we obtained at each time-step of the integration a polar angle ϕ in a (ψ_1^S, ψ_2^S) plane rescaled so that the stable $\sigma = 180°$ point is at the origin. We then computed at each step of the numerical integration the dispersion D_ϕ, in the polar angle ϕ, defined as

$$D_\phi{}^2 = \frac{1}{N(N-1)} \sum_{i \neq j} (\phi_i - \phi_j)^2, \tag{7}$$

where $N = 40$ is the number of integrated bodies and ϕ_i is the polar angle of the ith body ($i = 1, \ldots, N$). Fig. 13 shows the time-behaviour of D_ϕ: since we started with a compact cluster, D_ϕ is initially small (≃5°), but grows with time because of the differential libration of the bodies in the resonance. After 2.5 Myr, it reaches the saturation level at 103°.0, which corresponds to a uniform distribution of bodies along a circle (Vokrouhlický et al. 2006, Carruba 2009b).[2] This result suggests that the Tina family is at least 2.5 Myr old, that is, about three times the anti-aligned libration oscillation period of (1222) Tina. The dispersion of D_ϕ on a time-scale of three libration oscillation periods is quite a typical result (Vokrouhlický et al. 2006; Carruba 2009b).

In the next section, we will investigate a better constraint on the family age that comes from the diffusion in the semimajor axis caused by the Yarkovsky and YORP effects.

6.2 Monte Carlo simulations

In this section, we will analyse the semimajor axis evolution of the Tina family members for the classical and frequency cases. The methods used here follow the work of Vokrouhlický et al. (2006a,b) that showed that the peculiar a-distribution of some asteroid families can be explained as a consequence of the combination of the Yarkovsky and YORP effects. In essence, the YORP effect forces the spin axes of asteroids to evolve towards the direction perpendicular to the orbital plane. In this configuration, the semimajor axis drift caused by the Yarkovsky effect is maximized. Asteroids either drift towards smaller a (if their rotation is retrograde) or larger a (if their rotation is prograde). This depletes the centre of the family in the semimajor axis distribution.

The family's final semimajor axis distribution resulting from this evolution depends on its initial velocity dispersion (parametrized by V_{EJ}; see equation 4), its age (Age), as well as on the YORP strength (C_{YORP}), which are all unknown a priori. To determine the values of these parameters, we proceed as follows: we fix a set of values of the parameters and we compute the expected final distribution of semimajor axes. The latter is then transformed into a one-dimensional distribution by computing for each body the parameter C using the following equation:

$$0.2H = \log_{10}\left(\frac{\Delta a}{C}\right), \tag{8}$$

where H is the absolute magnitude of the body and $\Delta a = a - a_c$ is the difference between its semimajor axis and the value a_c characterizing the centre of the family (i.e. its barycentre). The distribution of the values of C for the simulated family, $N(C)$, is then compared to that for the real family, $N_{obs}(C)$. We computed the number of objects for C-interval, using 20 intervals in C, starting from $C = -2 \times 10^{-5}$ with a step $\Delta C = 2 \times 10^{-6}$. The quality of the match between the two distributions is quantified by computing the χ^2-like value:

$$\psi_{\Delta C} = \sum_{\Delta C} \frac{[N(C) - N_{obs}(C)]^2}{N_{obs}(C)}. \tag{9}$$

We finally search for the values of the parameters that minimize $\psi_{\Delta C}$, that is, fit best the observed semimajor C-distribution of the family. More detail on the procedure outlined here can be found in Vokrouhlický et al. (2006a,b) and Carruba (2009a). We do not consider the effects of low-energy collisions (Dell'Oro & Cellino 2007), because Carruba (2009a) showed that they play at best a minor role with respect to the semimajor-axis evolution caused by the Yarkovsky and YORP effects.

[2] The current value of D_ϕ for the Tina family members is 96°.1.

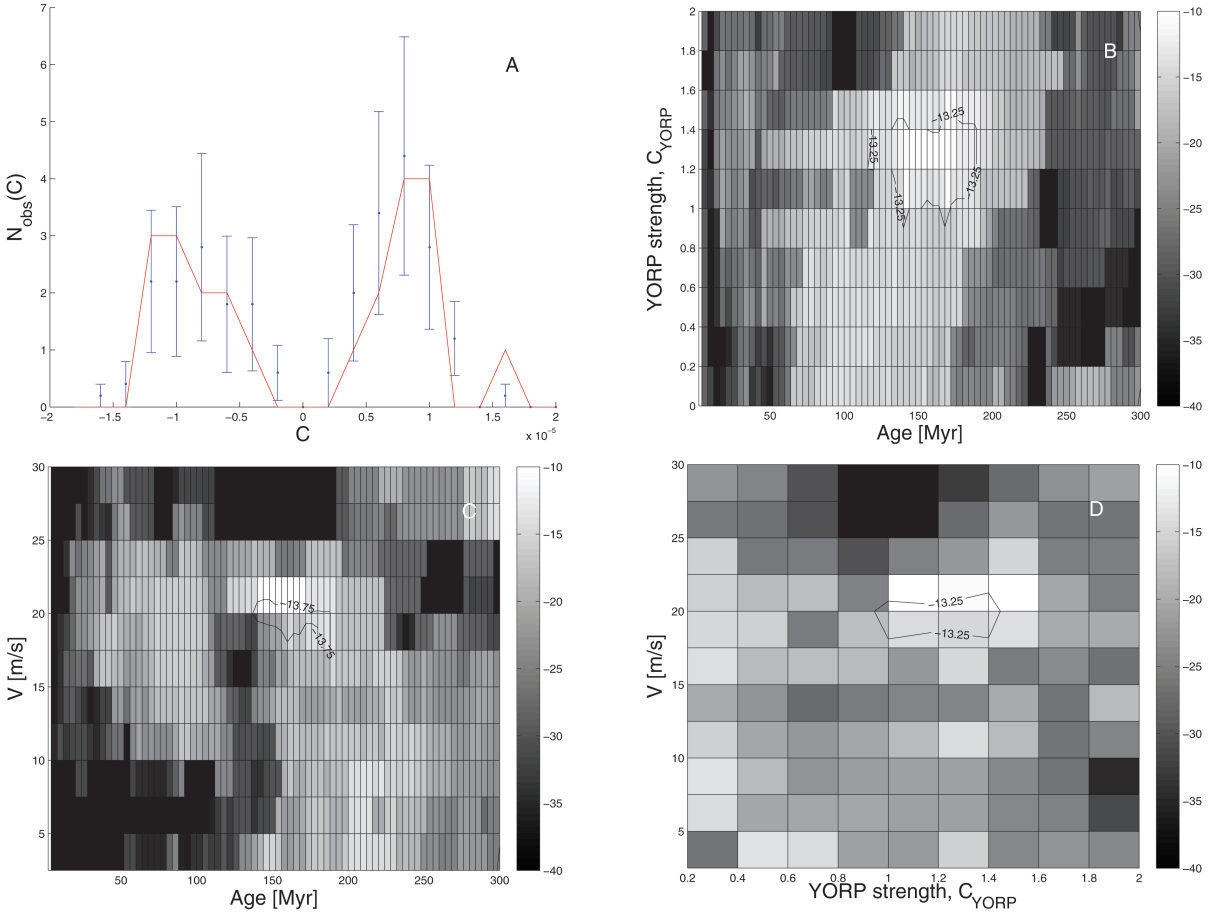

Figure 14. Panel A displays the best-fitting distribution $N(C)$ (red line) and the observed distribution $N_{\rm obs}(C)$ (in blue) for the classical family. The other panels show the values of the target function, $\psi_{\Delta C}$, in the (Age, $C_{\rm YORP}$) plane (panel B), in the (Age, V) plane (panel C) and in the ($C_{\rm YORP}$, V) plane (panel D). For these maps, in each cell, we report the minimal value of $\psi_{\Delta C}$ over the hidden dimension.

6.2.1 Fitting the semimajor-axis distribution: the classical family

We start by computing $N_{\rm obs}(C)$ for the classical family of Tina. This function depends on the adopted value for the family barycentre, $a_{\rm c}$, which is not very precisely determined. So, following Vokrouhlický et al. (2006a,b), we computed $N_{\rm obs}(C)$ as the average of the C-distribution for $a_{\rm c}$ in the interval (2.790, 2.794). The result is shown in Fig. 14 (panel A).

The other panels of Fig. 14 show the values of the target function $\psi_{\Delta C}$ in the (Age, $C_{\rm YORP}$) plane (panel B), in the (Age, V) plane (panel C) and in the ($C_{\rm YORP}$, V) plane (panel D).[3] Since there were 20 intervals in C, we used a value of $\psi_{\Delta C}$ of 13.25 as a limit for an acceptable fit, as this would correspond to a probability of 95 per cent that the simulated distribution is equivalent to the observed (Press et al. 2001).

From this analysis, we obtain the following best-fitting solution for the age, T, the characteristic ejection velocity field, $V_{\rm EJ}$, and the YORP strength ($C_{\rm YORP}$): $T = 170^{+20}_{-30}$ Myr, $V_{\rm EJ} = 20.0^{+1.0}_{-2.5}$ m s^{-1} and $C_{\rm YORP} = 1.00^{+0.45}_{-0.10}$. Note that the estimate of the initial velocity dispersion of the family is in perfect agreement with that obtained in Section 5. This is remarkable, because the two methods used in Section 5 and here are truly independent.

[3] To associate lower levels of $\psi_{\Delta C}$ with whiter tones, we plotted colour plots of $-\psi_{\Delta C}$.

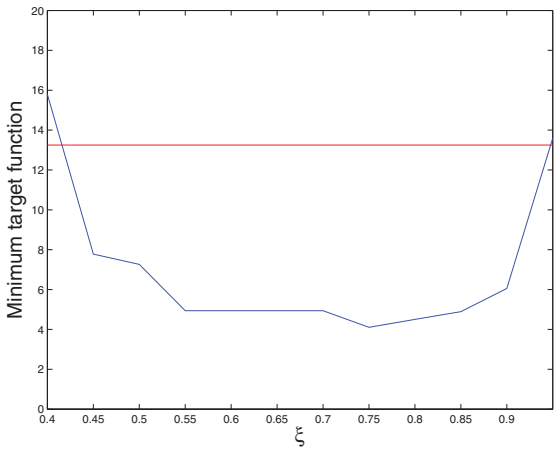

Figure 15. Minimum values of the target function $\psi_{\Delta C}$ as a function of the asymmetry parameter ξ for the classical family.

Following the Vokrouhlický et al. (2006b) approach, we introduced the fourth parameter, ξ, which yields the fraction of initially prograde rotating asteroids. Fig. 15 displays minimum values of the target function, $\psi_{\Delta C}$, for different values of the asymmetry parameter, ξ, characterizing the initial proportion of the prograde versus the retrograde rotating fragments. As also found in Vokrouhlický et al. (2006b) for the Agnia family and by Carruba (2009a) for the Padua

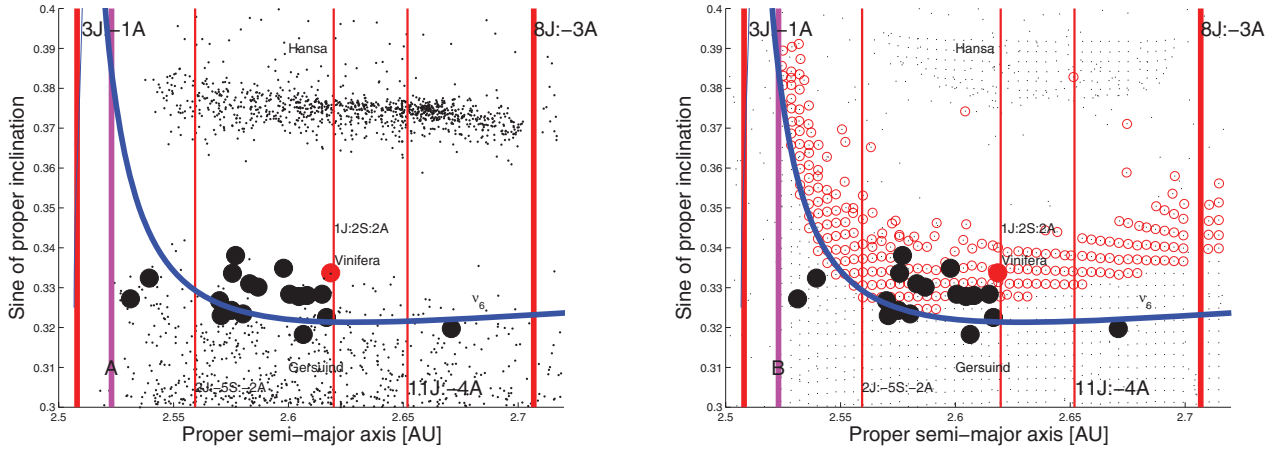

Figure 16. Panel A: an $(a, \sin(i))$ projection of the asteroids in the region around (759) Vinifera. Panel B: an $(a, \sin(i))$ projection of averaged elements of test particles in the region of (759) Vinifera.

family, the Tina family also seems to be characterized by an asymmetry between the prograde and retrograde rotators. The fraction of initially prograde rotating asteroids, ξ, is, however, poorly constrained: we found a value of $\xi = 0.75^{+0.20}_{-0.33}$, which seems to indicate a prevalence of prograde rotating asteroids, but it is also compatible with a balanced distribution or even with a slight prevalence of initially retrograde rotating asteroids.

Concerning the frequency family, we repeated the Monte Carlo analysis and the results are in very good agreement with those of the classical family. We found an Age $= 160^{+20}_{-30}$ Myr, $V_{\rm EJ} = 20.0^{+1.0}_{-2.5}$ m s^{-1}, $C_{\rm YORP} = 1.0^{+0.1}_{-0.1}$ and $\xi = 0.55^{+0.17}_{-0.08}$.

7 (759) VINIFERA

Until recently, the only other asteroid that was known to be in an anti-aligned librating state of the ν_6 resonance was (759) Vinifera (Froeschlé & Scholl 1987). Fig. 16 (panel A) displays an $(a, \sin(i))$ projection of the asteroids in the region of (759) Vinifera. The latter is identified by a red full dot, whereas the other 18 anti-aligned librating asteroids in the region are shown as full black dots in Fig. 16. At the moment, no dynamical family was found around (759) Vinifera (Carruba 2010b), nor around any of the other librating asteroids. A small clump with 10 members around (59494) 1999 JN5 is identifiable in the domain of proper frequencies (n, g, $g + s$), but this number is below the minimum one required for statistical significance (22 members, Carruba 2010b).

One may wonder why there is no family in the region of (759) Vinifera. Is this due to dynamical causes, such as the dimension of the region of anti-aligned libration in the vicinity of the asteroid, or simply is it just a consequence of the fact that (759) Vinifera was never broken up by a collision? To investigate the dimension of the anti-aligned librating island, we integrated with SWIFT_MVSF 2200 particles for 20 Myr, with initial conditions chosen on a regular 55 by 40 grid in the $(a, \sin(i))$ plane. We used a resolution in a of 0.004 au and in i of 0.2. Our particles covered a range 2.500–2.716 au in a and 16.0–23.8 in i. The initial values of e and of the angular elements Ω, ω, and λ of the test particles were set equal to those of (759) Vinifera.

Fig. 16 (panel B) shows the averaged elements of test particles in the $(a, \sin(i))$ plane. The blue line shows the location of the secular resonance centre in the region, as computed by the analytical theory of Milani & Knežević (1994). Red circles identify the location of anti-aligned librators. The reader may note that the anti-aligned librating region covers a smaller range of inclination values with respect to the same region near Tina (see Fig. 5, panel B). To investigate the dynamical stability of asteroids in the (759) Vinifera region, we studied the dynamical evolution of the (59494) frequency clump when the Yarkovsky effect is considered, as well as of all the 18 ν_6 anti-aligned librating asteroids in the region. We used typical Yarkovsky parameters of S-type objects, which is consistent with the taxonomy of asteroids in the region (Carruba 2010b), and the same set-up as used for the Yarkovsky integrations of Tina members (see Section 4.2). We observed that the group around (59494) dispersed in less than 2 Myr and should therefore not be considered statistically significant. Concerning the anti-aligned asteroids in the (759) Vinifera region, with the exception of two objects, (109429) (2001 QQ195) and (2000) QV14, which switched to circulating states before the end of the integration, all the other 16 initially anti-aligned asteroids remained in librating states for the whole length of the integration (300 Myr). Thus, we conclude that putative (759) Vinifera families in anti-aligned libration orbits could remain identifiable for a time-scale of at least 300 Myr. In conclusion, the fact that we do not observe them can be due to either of the following two reasons: (i) there has been no collisional break-up in the last 300 Myr; or (ii) there is a family of small objects but the latter has not yet been detected. A more complete asteroid catalogue in the region is therefore needed before drawing a conclusion on this subject.

8 CONCLUSIONS

In this work:

(i) We investigated the dynamics of the Tina family, which is, so far, the only asteroid family completely embedded in a secular resonance (i.e. all family members are in resonant libration). Contrary to the case of the Agnia and Padua families in the z_1 resonances, members of the Tina families that escape from the ν_6 anti-aligned libration island are unstable on time-scales of up to 10 Myr because of close encounters with Mars and other terrestrial planets, which explains why no Tina members are currently found outside the stable island.

(ii) We defined and computed ν_6 resonant proper elements in two different ways for the family members.

(iii) We obtained dynamical maps for the Tina region and investigated the long-term orbital evolution of Tina members when the Yarkovsky effect is considered. Anti-aligned librators cannot reach Mars-crossing eccentricities and are not destabilized unlike ν_6 circulators and aligned librators in the region. As a consequence, the Tina family resides in a stable island of motion.

(iv) We used the $K_2' = \sqrt{1-e^2}(1-\cos i)$ conserved quantity of the ν_6 resonance to set constraints on the original ejection velocities of Tina family members. Current values of K_2' are compatible with an original value of $V_{\rm EJ}$ (see equation 4) of $22.5 \pm 5.0\,{\rm m\,s^{-1}}$.

(v) We put constraints on the family age (170^{+20}_{-30} Myr) and on the initial velocity dispersion ($20^{+1}_{-2.5}\,{\rm m\,s^{-1}}$).

(vi) We studied the case of the other large anti-aligned librating asteroid in the region, (759) Vinifera, and briefly discussed why it is not associated to any known family.

A natural question that now arises is on the nature of the Tina family. Since all its members seem to lie in a stable island, they could be, in principle, just asteroids that happened to survive in this stable dynamical niche. Information on the taxonomy of family members could help solve this problem, but, unfortunately, this information is only available for (1222) Tina itself (Carruba 2010b). Six objects in the region have SDSS-MOC3 flux data that are compatible with an S-complex composition, but this is clearly not enough to reach a definitive conclusion on the genetic link between the family members and more data need to be collected.

An interesting issue for future research is the response of anti-aligned librators to giant planet migration. Giant planet migration causes the ν_6 resonance to sweep through the asteroid belt from larger to smaller semimajor axes. It will be interesting to investigate whether objects in anti-aligned libration configuration could have been captured in this dynamical state during the phase of secular resonance sweeping and under which conditions. Coupled with other existing constraints on giant planet migration, this study could therefore lead to a better characterization of the real dynamical evolution that the planets had at the time they cleared the planetesimal disc from their vicinity.

More important than the real status of the Tina family as an actual collisional group and the possible lines of research that may arise from it is, however, the discovery of a new kind of resonant dynamical family. The identification of the first ν_6 anti-aligned librating family is, in our opinion, an interesting result in orbital dynamics, which further emphasizes the vitality of asteroid dynamics as a field of research.

ACKNOWLEDGMENTS

We thank the reviewer of this paper, David Vokrouhlický, for careful revision of this paper and his fruitful comments that significantly improved its quality. We would like to thank the São Paulo State Science Foundation (FAPESP) that supported this work via the grant 06/50005-5 and the Brazilian National Research Council (CNPq, grants 302183/2008-6 and 473345/2009-9). VC is also grateful to the Department of Mathematics of FEG-UNESP for the use of their facilities.

REFERENCES

Bendjoya Ph., Zappalà V., 2002, in Bottke W. F., Jr, Cellino A., Paolicchi P., Binzel R. P., eds, Asteroids III. Univ. Arizona Press, Tucson, p. 613
Brož M., 1999, Thesis, Charles Univ., Prague, Czech Republic
Brož M., Vokrouhlický D., 2008, MNRAS, 390, 715
Carruba V., 2009a, MNRAS, 395, 358
Carruba V., 2009b, MNRAS, 398, 1512
Carruba V., 2010a, MNRAS, 403, 1834
Carruba V., 2010b, MNRAS, 408, 580
Carruba V., Michtchenko T., 2007, A&A, 475, 1145
Carruba V., Michtchenko T., 2009, A&A, 493, 267
Carruba V., Burns J. A., Bottke W., Nesvorný D., 2003, Icarus, 162, 308
Carruba V., Michtchenko T., Roig F., Ferraz-Mello S., Nesvorný D., 2005, A&A, 441, 819
Charlier C. V. L., 1902, Die Mechanik des Himmels, 410-413. Verlag von Veit & Co., Leipzig
Dell'Oro A., Cellino A., 2007, MNRAS, 380, 399
Farinella P., Vokrouhlický D., Hartmann W. K., 1998, Icarus, 132, 378
Froeschlé Ch., Scholl H., 1987, A&A, 179, 294
Knežević Z., Milani A., 2000, Celest. Mech. Dyn. Astron., 78, 17
Knežević Z., Milani A., 2003, A&A, 403, 1165
Levison H. F., Duncan M. J., 1994, Icarus, 108, 18
Milani A., Knežević Z., 1992, Icarus, 98, 211
Milani A., Knežević Z., 1994, Icarus, 107, 219
Morbidelli A., 2002, Modern Celestial Mechanics: Aspects of Solar System Dynamics. Taylor & Francis, London
Morbidelli A., Henrard J., 1991, Celest. Mech. Dyn. Astron., 51, 169
Nesvorný D., Vokrouhlický D., 2006, AJ, 132, 1950
Press V. H., Teukolsky S. A., Vetterlink W. T., Flannery B. P., 2001, Numerical Recipes in Fortran 77. Cambridge Univ. Press, Cambridge
Vokrouhlický D., Brož M., Bottke W. F., Nesvorný D., Morbidelli A., 2006a, Icarus, 182, 118
Vokrouhlický D., Brož M., Bottke W. F., Nesvorný D., Morbidelli A., 2006b, Icarus, 183, 349
Williams J. G., 1969, PhD thesis, Univ. of California, Los Angeles
Zappalà V., Bendjoya Ph., Cellino A., Farinella P., Froeschlé C., 1995, Icarus, 116, 291

This paper has been typeset from a TEX/LATEX file prepared by the author.